Lab on a Chip

Cite this: *Lab Chip*, 2012, **12**, 3117–3126

www.rsc.org/loc

PAPER

Heterotypic cell pair co-culturing on patterned microarrays†

Edward J. Felton,[a] Craig R. Copeland,[a] Christopher S. Chen[b] and Daniel H. Reich[a]

Received 26th August 2011, Accepted 9th May 2012
DOI: 10.1039/c2lc40349h

We present a pair-wise co-culturing technique that creates large numbers of heterotypic cell pairs in patterned arrays. Lithographic patterning produces arrays with thousands of traps, each designed to accommodate only two cells and confine them at these sites for co-culturing. Two variants are introduced: a random seeding method that sediments a mixture of two cell types onto the array, and an approach that incorporates ferromagnetic thin films into the arrays and attracts cells that have been attached to ferromagnetic nanowires to the array sites through dipole interactions. The array technique includes the utilization of custom image analysis software that extracts data from multi-channel fluorescence images and records information about the cells in every trap, enabling the acquisition of accurate, high-statistics data. The applicability of the technique was demonstrated in experiments examining proliferation rates in pairs of bovine pulmonary artery endothelial and smooth muscle cells. Results demonstrated that heterotypic interactions favored smooth muscle cell proliferation while disfavoring endothelial cell proliferation. This is one example of a variety of cell-cell interactions that could be probed with this method.

1 Introduction

Interactions between cells play a vital role in a variety of cell processes. Accordingly, the ability to control the organization and spatial positioning of cells is crucial in experiments that investigate effects mediated by these interactions. To this end, a number of approaches have been established to create arrays of patterned cells. One such approach employs micropatterning to promote cell adhesion in particular areas of the substrate with adhesive ligands, while rendering other regions non-adhesive to prevent cell attachment. Cell patterning then occurs passively through trapping *via* cell-substrate adhesive interactions.[1–4] Cells have also been actively manipulated into patterns by several methods, including magnetic forces,[5–8] magnetophoresis,[9] dielectrophoresis,[10,11] microfluidics,[12,13] and with optical tweezers.[14,15]

One potential use of such patterns is to study interactions between cells in a pairwise configuration, in which contact between cells is made in a controlled manner and the pairs are isolated from the influences of other cells. Homotypic cell pairs have been produced by seeding cells on micropatterned arrays of adhesive islands designed to accommodate two cells,[16] and dielectrophoresis has also been used to form isolated cell pairs.[17,18] These studies have shown that such cell-cell interactions can influence cell structure, polarity, and proliferation.[19–21] In addition to pair interactions of cells of a single type, cell-cell communication between cells of different types has been shown to affect cell behavior.[22,23] Thus, generating heterotypic cell pairs, comprised of two cells of different types, would enable additional investigations of these interactions.

The creation of heterotypic pairs poses additional challenges, and to date, studies of heterotypic cell interactions have primarily focused on approaches that involve large numbers of cells rather than individual pairs. These include cells mixed in co-culture,[24,25] as well as methods that physically separate the cell types by culturing the two types on opposite sides of a membrane[26–28] or segregate them into different regions of the same substrate by controlling cell attachment at different times.[29,30] For cells in configurations with many other cells it is difficult to control the area in which a given cell can spread as well as the number of neighboring cells contacting it, both of which are known to influence cell functions. For example, proliferation is positively correlated with increased cell spreading, and has been shown to vary with the relative number of cells present in bulk co-cultures[31] and with the number of cells contacting a particular cell in a controlled microenvironment.[32] These parameters may be more easily controlled for cells in heterotypic pairs, and more recently attention has been focused on developing approaches that form such pairs.[12,18,33–35]

Here, we introduce a robust technique to create micropatterned arrays of cells for use in cell interaction studies. Rectangular arrays of holes, herein referred to as traps, are patterned into gold thin films *via* standard lithography, exposing the underlying glass substrate. The area of the traps is chosen to allow for occupation by two cells, and a mixture of two cell types is added to the array *via* sedimentation. Chemical patterning is employed to allow attachment only in the traps and to confine

[a]*Department of Physics and Astronomy, The Johns Hopkins University, Baltimore, MD 21218 E-mail: reich@jhu.edu*
[b]*Department of Bioengineering, University of Pennsylvania, Philadelphia, PA 19104*
† Electronic supplementary information (ESI) available. See DOI: 10.1039/c2lc40349h

the cell pairs to those sites.[36] This technique offers several advantages. Fabrication of the arrays is simple, requiring only single-step microlithography and wet chemical etching, and allows for patterning over large areas that results in arrays of thousands of traps and yields large numbers of cell pairs. Each array contains heterotypic and homotypic pairs, as well as single cells. The shape of the traps and lattice spacing of the array may be controlled as desired by designing the mask accordingly. Furthermore, the chemical treatment of the arrays acts to prevent cells in a trap from migrating, and forces them into contact with each other. The area of the individual traps can also be adjusted for use with particular cell types. In this work, we apply this technique to produce pairs using endothelial and smooth muscle cells that reside in close proximity, and demonstrate the use of the arrays of cell pairs to conduct proliferation studies of cells making contact in this configuration.

In addition, we have developed and incorporated into this system an enhanced method for producing heterotypic cell pairs that uses magnetic forces to guide cells to the traps' ends. The arrays used with this approach include magnetic metal films beneath the gold layer. Magnetizing these films yields magnetic poles at opposite ends of each trap, which are analogous to the poles at the ends of lithographically patterned micromagnets used previously to position cells.[5] Rod-shaped ferromagnetic particles are bound to the cells, and while in suspension are oriented with an external field. In this configuration, the magnetic rods are attracted to one of the poles and repulsed by the other, and thus the cells they are bound to are selectively guided to one end of the traps. We demonstrate the use of this magnetic interaction to form heterotypic pairs by adding the two cell types sequentially and changing the external field's orientation to direct the different cell types to opposite ends of the traps, as illustrated in Fig. 1. The magnetic rods with the first cell type align with an external field applied perpendicularly to the substrate, and are attracted to the north pole (Fig. 1(a)). The orientation of the field is reversed before the second cell type is added, trapping these cells at the south pole (Fig. 1(b)), resulting in a heterotypic pair (Fig. 1(c)). We have used this magnetically enhanced approach to create heterotypic pairs of endothelial and cancer cells.

The technique described here traps cells at thousands of array sites, introducing the challenge of thoroughly analyzing the whole array. To do so we have developed a flexible, software-based analysis procedure to record the results from every trap in an array, rather than basing results on a representative sampling. This approach gives the ability to derive high-statistics quantitative data from the large numbers of traps in our arrays, and is adaptable for use with a range of image magnifications. A brightfield image is used to locate the traps and a fluorescent nuclear stain is used to record the location of each cell. Additional fluorescence channels are available to label particular objects and cell structures of interest. As an example, we use a cytoplasm stain to identify cell type, and a nucleic acid stain to label the nuclei of proliferating cells. After the software has been used to process the images, it further allows the user to inspect and make changes to its determinations, ensuring a high degree of accuracy. The use of this analysis tool, in combination with the ability to create large numbers of cell pairs, enables the production and analysis of large data sets from experiments probing a variety of cell functions and behaviors influenced by interactions between cells.

2 Materials and Methods

2.1 Sample Fabrication and Characterization

Thin metallic films consisting of a 2.5 nm chromium adhesion layer followed by 30 nm of gold were thermally evaporated on acid-cleaned microscope slides. Rectangular arrays of elliptically shaped holes in the thin film were then created by contact

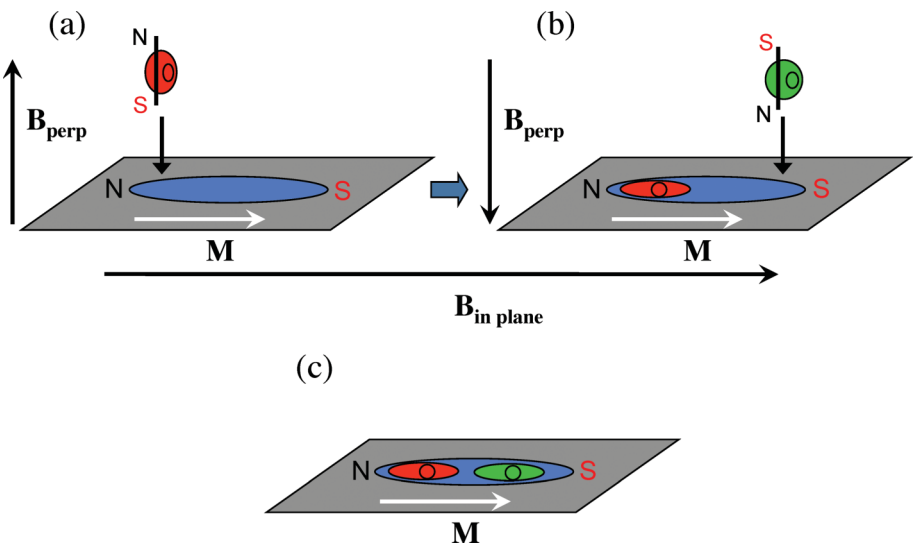

Fig. 1 Schematic of magnetic trapping, with array magnetization **M** in the direction of the traps' major axes. (a) Suspended cells with attached nanowires align with an applied perpendicular magnetic field **B** and are attracted to the north pole of the trap *via* dipole interactions. (b) After these cells adhere to the substrate the orientation of the applied field is reversed. The second cell type is introduced, and the cells with attached nanowires again align with the applied field but are now attracted to the traps' south pole. (c) Once the second cell type attaches to the substrate the external field is removed.

photolithography and chemical etching with gold (GE-8148, Transene, Danvers, MA) and chromium (Cyantek, Fremont, CA) etchants. Arrays were fabricated with two trap sizes, denoted here by their minor and major axes, and by the center-to-center spacings between traps. The smaller traps we employed were 14 × 70 μm^2, with spacings of 150 μm along the ellipses' major axes and 94 μm along their minor axes. These arrays were comprised of 5,400 traps. Larger traps were 24 × 80 μm^2, and had spacings of 160 μm along the ellipses' major axes and 104 μm along their minor axes. Arrays of larger traps consisted of 4,480 traps. Square samples with two small-trap and two large-trap arrays were cut to fit 35 mm tissue culture dishes.

Thin films incorporating magnetic layers were deposited by magnetron sputtering. A 200 nm layer of permalloy ($Ni_{81}Fe_{19}$) was sputtered onto acid-cleaned glass, followed by 50 nm of gold. This was repeated to add a second 200 nm layer of permalloy and a final 50 nm layer of gold. Permalloy was chosen due to its ability to withstand exposure to phosphate buffered saline (PBS) and cell culture media, and two 200 nm thick layers were used (rather than a single thicker layer) to increase the films' remanent magnetization. Vibrating sample magnetometer measurements of the permalloy bi-layer films found the remanent magnetization to be 703 kA m^{-1}, 86% of the saturation magnetization, as seen in Fig. 2(a). Comparatively,

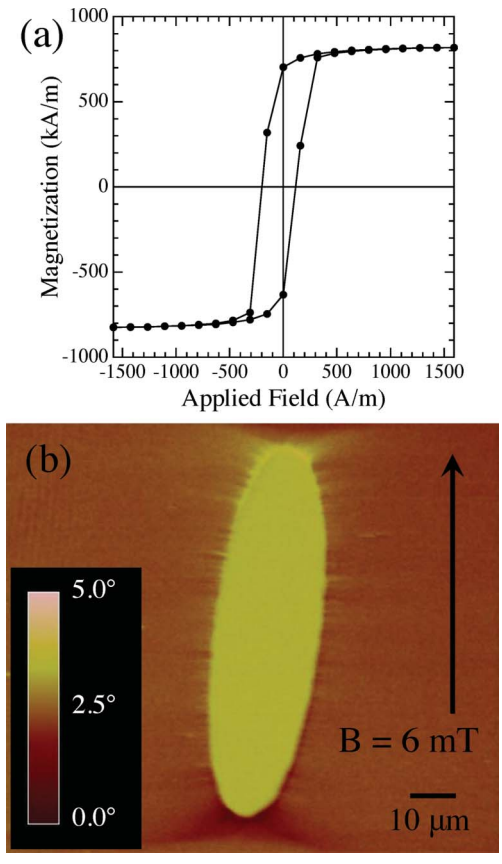

Fig. 2 (a) Magnetic moment *vs.* magnetic field for permalloy bi-layer thin film of two 200 nm permalloy layers separated by 50 nm of gold. (b) Magnetic Force Microscope phase measurement of a 24 × 80 μm^2 permalloy bi-layer trap with an in-plane field applied in the direction of the major axis.

400 nm single layer permalloy films had a similar saturation magnetization but remanent magnetizations of 62%.

Arrays of ellipses were formed *via* photolithographic patterning, after which gold etchant and 10% nitric acid were used alternately to etch through the four layers of material. Two trap sizes, each with two intertrap spacings, were used for magnetic arrays. 18 × 80 μm^2 traps had center-to-center spacings of either 156 μm along their major axes and 94 μm along their minor axes, or 216 μm along their major axes and 154 μm along their minor axes, and contained 4,000 and 1,750 traps, respectively. 24 × 80 μm^2 traps had center-to-center spacings of either 156 μm along their major axes and 100 μm along their minor axes, or 216 μm along their major axes and 160 μm along their minor axes, also containing 4,000 and 1,750 traps, respectively. Square samples with each of the four array types were cut to fit 35 mm tissue culture dishes.

For the rod-shaped ferromagnetic particles needed for the magnetic trapping, we used nickel nanowires. The nanowires were fabricated by electrochemical deposition in the cylindrical nanopores of 50 μm-thick alumina filter membranes (Anodisc, Whatman, Maidstone, UK) as described previously.[37] The wires' radius of 175 ± 20 nm was determined by the pore size, and their length of 30 μm was controlled by monitoring the deposition current. After deposition, the alumina was dissolved in 0.5 M KOH at 50 °C overnight to release the nanowires from the membranes. Once in suspension, the nanowires were collected with a magnet, rinsed in ethanol, and diluted in PBS to a lower concentration for use with cells. The nanowires were exposed to fields in excess of 0.3 T during magnetic collection, and due to their large magnetic shape anisotropy they remained magnetized with a remanent magnetization of 300 kA m^{-1}, which is 70% of their saturation magnetization.

Chemical patterning was used to prohibit cell adhesion on the samples outside the traps and to promote adhesion in the traps. Prior to use, arrays were submerged in 2 mM hexadecanethiol in ethanol for 15 min, during which the thiol groups attached to the gold surface. They were then rinsed in ethanol and dried with nitrogen. This was followed with a 0.2% w/v solution of Pluronic F-127 (Sigma-Aldrich, St. Louis, MO) in PBS that adhered to the hexadecanethiol to block cell attachment. After 30 min samples were rinsed with PBS, and 20 μg mL^{-1} fibronectin (Sigma-Aldrich) in PBS was then added for a minimum of one hour to promote cell adhesion in the traps. This solution was removed by repeated rinsing with cell culture media just before seeding cells onto the samples.

2.2 Cell Culture

NIH 3T3 mouse fibroblast and A-431 human skin carcinoma cells (both from American Type Culture Collection, Manassas, VA) were cultured in high glucose Dulbecco's Modified Eagle Medium (DMEM). Bovine pulmonary artery endothelial cells (BPAECs, VEC Technologies, Rennselaer, NY) and bovine pulmonary artery smooth muscle cells (BPASMCs, gift from D. E. Ingber, Harvard University) were cultured in low glucose DMEM. All media were supplemented with serum (3T3s and BPAECs with 5% bovine serum, BPASMCs with 10% bovine serum, and A-431s with 10% fetal bovine serum) along with 100 U mL^{-1} penicillin and 100 μg mL^{-1} streptomycin. A-431

media was supplemented with an additional 2 mM L-glutamine. All cells were incubated at 37 °C, with 3T3, A-431, and BPAEC cells in 5% CO_2 and BPASMCs in 10% CO_2. BPAEC/A-431 and BPAEC/BPASMC co-cultures were cultured in BPAEC media in 5% and 10% CO_2, respectively. All cell culture reagents were obtained from Invitrogen (Carlsbad, CA).

2.3 Random Seeding on Arrays

NIH 3T3 Cells. To test heterotypic pair formation using labeled 3T3 cells, two identically prepared dishes of cells were fluorescently labeled with different live-cell stains. One population was stained with CellTracker Green CMFDA, and the other with CellTracker Orange CMTMR (Invitrogen). Cells were labeled by incubating for 30 min in CellTracker stain diluted 1 : 2,000 in serum-free DMEM, after which the stain solution was replaced with growth media. After fluorescent staining, cells were detached from culture dishes by exposure to 0.25% trypsin with EDTA·4Na (Invitrogen), re-suspended in growth media, and diluted to 50,000 or 100,000 cells mL^{-1}. The two populations were mixed, 2 mL of the mixture were seeded onto non-magnetic gold arrays, and samples were incubated for 40 min to allow cell adhesion in the traps. Samples were then rinsed with media to remove unattached cells, incubated for an additional 80 min, and fixed with 4% paraformaldehyde (Electron Microscopy Sciences, Hatfield, PA) for 10 min. After rinsing 3 times with PBS, cell nuclei were stained with Hoescht 33258 (Invitrogen) diluted 1 : 2,000 in PBS for 20 min, after which samples were again rinsed in PBS and mounted with Fluoromount G (Electron Microscopy Sciences).

Arrays with randomly seeded 3T3 cells were also used in proliferation experiments to analyze software accuracy. For this case, one population was labeled with CellTracker Green, while the other was unlabeled. After staining, each type was diluted to approximately 100,000 cells mL^{-1}, and then mixed and seeded as described above. BrdU (GE Healthcare, Little Chalfont, UK) was added at 1 : 100 to samples as a proliferation-labeling agent for S phase entry once the rinse to remove unattached cells was performed. Samples were fixed 20 h after the addition of BrdU, rinsed 3 times in PBS, and treated for 20 min with a solution of 90% ethanol, 5% deionized water, and 5% acetic acid to permeablize the membranes and denature the nuclei. After rinsing 3 times in PBS, samples were exposed to a blocking solution of 33% goat serum (Invitrogen) in PBS for one hour. Samples were subsequently incubated for one hour with a monoclonal mouse *anti*-BrdU primary antibody (GE Healthcare) and then rinsed 3 times, incubated in PBS for 10 min, and rinsed another 3 times. Alexa Fluor 647 goat *anti*-mouse (Invitrogen) was used as a secondary antibody, diluted 1 : 200 in 33% goat serum, and samples were stained for one hour followed by rinsing 3 times in PBS. Staining of cell nuclei and sample mounting were done as described above.

BPAEC and BPASMC Cells. Experiments using BPAEC and BPASMC cells randomly seeded onto non-magnetic arrays were carried out to measure cell proliferation in cell pairs. The cells were synchronized to G_0 before use by holding BPAEC and BPASMC cultures at confluence for 96 and 48 h, respectively, in growth media. To distinguish between the two cell types, the BPAECs were fluorescently labeled after synchronization with either CellTracker Green or CellTracker Orange, while the BPASMCs were not stained, and each type was diluted to approximately 100,000 cells mL^{-1} before mixing. Cell seeding, BrdU addition, fixation, and post-fixation processing were carried out as described above. For samples with CellTracker Orange-stained BPAECs, Alexa Fluor 647 goat *anti*-mouse (Invitrogen) was used as a secondary antibody; for samples with CellTracker Green-stained BPAECs, Alexa Fluor 594 goat *anti*-mouse (Invitrogen) was used.

2.4 Magnetic Trapping

3T3 mixtures or BPAEC and A-431 cells were used in trapping experiments with magnetic arrays, and were attached to nickel nanowires *via* overnight incubation with cells in culture, as described previously.[5] Cell labeling was performed as described above. For 3T3 cells, two identical dishes of cells with nanowires were labeled with CellTracker Green and Orange before use. For BPAEC and A-431 cells, BPAECs were labeled with CellTracker Green while A-431s remained unlabeled. Cells were then detached from the culture dishes with trypsin-EDTA, and re-suspended in media. The nanowires remained bound to cells despite exposure to trypsin, and cells without attached nanowires were removed with a single-pass magnetic separation.[37] The cells with nanowires were then adjusted to final concentrations of 50,000–200,000 cells mL^{-1} before use. We have previously demonstrated in manipulations of this type that the nanowires are not toxic to cells in culture on the timescale of several days.[37]

Prior to chemical functionalization, exposure to the face field of a rare earth magnet (> 0.2 T) magnetized the permalloy array samples in the direction of the ellipses' major axes, creating magnetic poles at the ends of the traps. An in-plane field of 2.5 mT was applied to further magnetize the arrays and increase the strength of the magnetic poles during the cell trapping process. A magnetic force microscope image of a 24 × 80 μm^2 magnetic trap with a 6 mT in-plane field applied along the major axis is shown in Fig. 2(b). The bright and dark regions visible at opposite ends of the trap correspond to magnetic poles, confirming that the trap is magnetized.

To form heterotypic pairs, a 3.5 mT uniform magnetic field was first applied perpendicularly to the plane of the arrays, and 2 mL of one cell type were added. The nanowires aligned with the perpendicular field and were selectively attracted to one pole of the traps through magnetic dipole forces, as depicted schematically in Fig. 1(a). After incubation for 30–45 min, the arrays were rinsed with media to remove unattached cells, and the perpendicular field was reversed before seeding 2 mL of the second cell type. The nanowires with these cells aligned with the reversed field and were selectively trapped at the opposite poles (Fig. 1(b)). The arrays were again rinsed with media after 30–45 min, and then incubated for 2 h, resulting in heterotypic pairs confined within the traps as shown in Fig. 1(c). After fixing in 4% paraformaldehyde for 10 min, the nuclei were stained with Hoescht 33258, and the samples were then mounted. The magnetic fields applied during the trapping process were small in magnitude, and while very large magnetic fields (above 8 T) have been shown to affect cells,[38,39] no such effects were observed in our experiments.

2.5 Imaging and Data Acquisition

Arrays were manually imaged on a Nikon TE2000 inverted microscope with a Photometrics Coolsnap HQ camera, using a 4X or 10X objective that captured up to 225 or 36 traps per image, respectively. A brightfield and three fluorescence images were acquired at each location.

3 Results and Discussion

3.1 Heterotypic Pair Formation

Random Seeding with 3T3 Cells. Green- and orange-labeled 3T3 cells were mixed and seeded onto non-magnetic gold arrays to form heterotypic pairs. A typical result of 3T3 pair formation is shown in Fig. 3, which displays images from an array of 24 × 80 μm^2 traps. Fig. 3(a) is a 10X fluorescence image of the cell nuclei in a 16 trap region. Traps with cell pairs as well as single cells and empty traps are present, and due to the chemical functionalization the cells are located only in the traps. A composite of the green and orange fluorescence cytoplasm stain images corresponding to this region is shown in Fig. 3(b), allowing for identification of heterotypic pairs as well as homotypic pairs and single cells of each type. The heterotypic pairs are highlighted. A 10X composite fluorescence image of a single heterotypic pair is shown in Fig. 3(c), in which the contact between the two cells confined to the trap is evident.

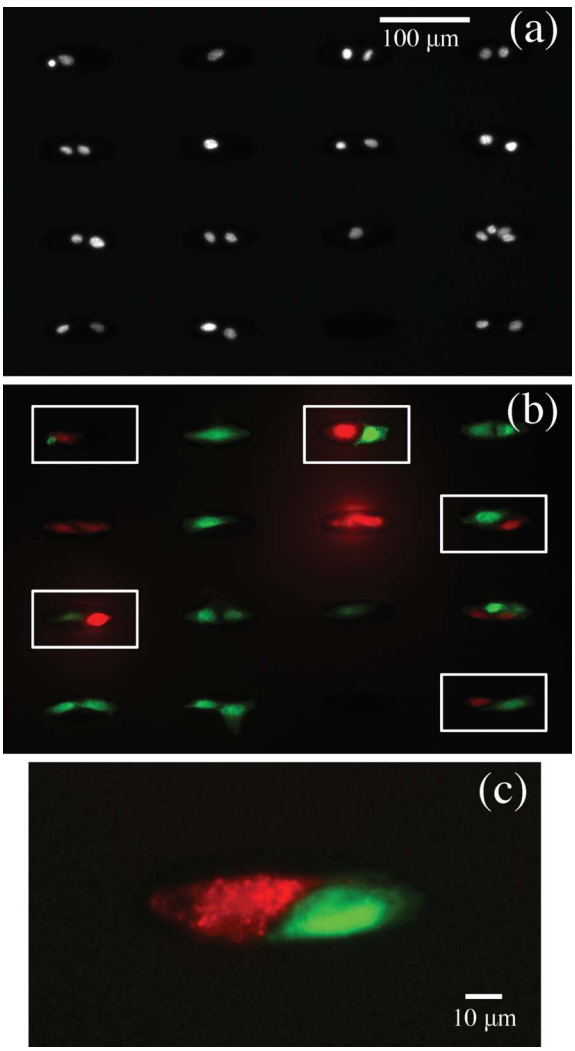

Fig. 3 10X images of NIH 3T3 fibroblast cells randomly seeded onto an array of 24 × 80 μm^2 traps. (a) Fluorescently labeled nuclei. (b) Composite of the green and orange cytoplasm label images. Traps with heterotypic pairs are highlighted. (c) Composite image of a single heterotypic pair.

Magnetic Trapping with 3T3 Cells. Green- and orange-labeled 3T3 cells with attached nanowires were magnetically trapped on permalloy arrays. Images of whole arrays were acquired at 4X magnification, and our analysis software was used to record the location (as determined by the nucleus' position) and type of the trapped cells. Manual inspection and correction of mistakes ensured accuracy. Fig. 4(a) displays a composite of the green and orange fluorescence images of a segment of one frame, in which

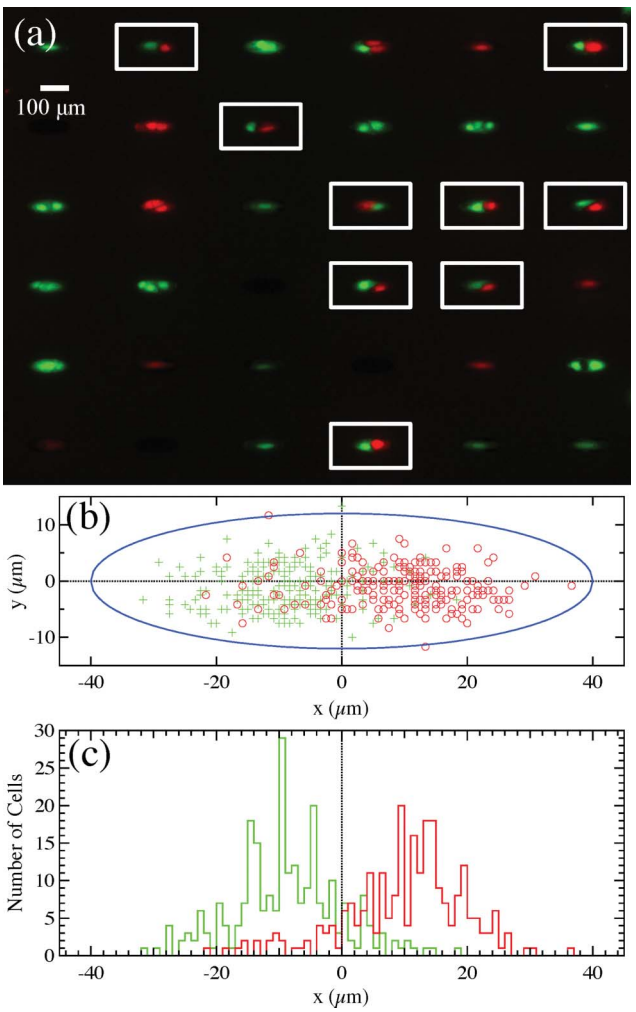

Fig. 4 (a) 10X composite fluorescence image of green and orange-labeled NIH 3T3 fibroblast cells with attached nanowires magnetically trapped on a permalloy array. Traps with heterotypic pairs are highlighted. (b) Locations of the nuclei of cells in heterotypic pairs for an array, indicating preferential trapping of the two cell types to opposite ends of the traps. (c) Histogram of the location along the major axis of the traps for the two cell types.

the heterotypic pairs are highlighted. We note that in heterotypic pairs, the green cells are predominantly located to the left and the orange cells are found to the right. A plot of the coordinates of the green and orange cells from the 245 heterotypic pairs in the array represented in Fig. 4(a) is displayed in Fig. 4(b), in which it is clear that the two cell types were selectively guided to opposite ends of the traps by magnetic forces. A histogram of the positions of these cells along the major axis of the traps is shown in Fig. 4(c), and the majority of the green and orange cells are located to the left and right of the origin, respectively. This trend is not present in histograms of randomly seeded cells.

Measurements of the coordinates of cells in traps containing just one cell (supplemental Fig. S1†) show that such cells were predominantly located near the centers of the traps. While they may have initially been selectively trapped at one pole, the cells' interaction with the substrate upon adhesion is stronger than the magnetic interaction force, and the cells are able to move within the traps and spread to fill the available area. The presence of a second cell, however, prevents either cell from spreading beyond its half, resulting in the cell positions seen in Fig. 4.

3.2 Software Analysis

Custom analysis software written with Igor Pro (WaveMetrics, Lake Oswego, OR) was used to extract data from the images. To illustrate this procedure, 10X brightfield and fluorescence images of a single trap from a 3T3 proliferation experiment are shown in Fig. 5. The traps are clear areas in an otherwise opaque substrate, and their locations are obtained by thresholding the brightfield image, with a particle analysis routine recording their coordinates and perimeters. The result is seen in Fig. 5(a), in which the yellow perimeter line is overlaid on the brightfield image. The coordinates of each trap are used to define rectangular regions of interest slightly larger than the traps for use with the fluorescence images.

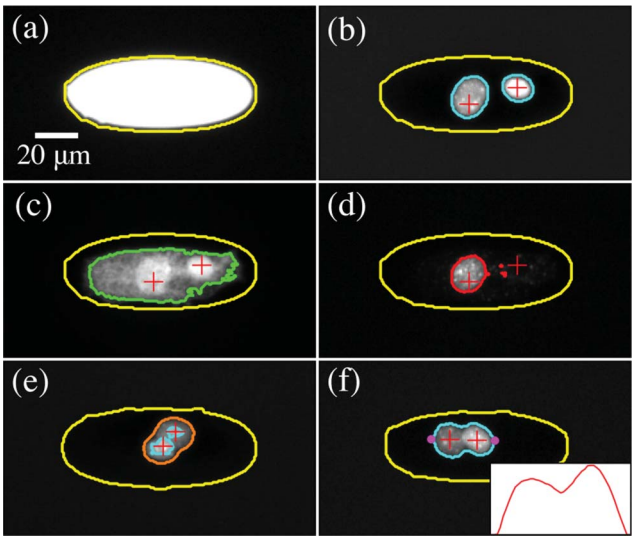

Fig. 5 10X images of NIH 3T3 fibroblasts in 24 × 80 μm^2 traps with overlays indicating determinations made by the analysis software. (a) Brightfield image with trap perimeter location. (b) Fluorescence image of nuclear label indicating presence of two cells. (c) Fluorescence image of green cytoplasm stain, showing that both cells in the trap are of the type labeled green. (d) Fluorescence image of the infrared BrdU label, indicating that only one cell was proliferating. (e) Fluorescence image of nuclear label for a trap with two nuclei close together. Only one object is found after the initial thresholding step, indicated by the orange outline, but additional thresholding identifies the object as two nuclei, as seen by the blue outlines. (f) Fluorescence image of nuclear label for another trap with two nuclei for which the thresholding technique evaluated the object and identified it as a single nucleus (blue boundary). The line profile technique then examined the intensity of the object along the line between the magenta points and found that two nuclei are present. The image intensity along this line is seen in the inset.

The nuclear-stain fluorescence image is shown in Fig. 5(b). An incremental thresholding process is performed within each trap's region of interest to find the number and location of the nuclei. The initial threshold level is determined by fitting a Gaussian curve to a histogram of the pixel intensities, and since the region is mostly dark the peak corresponds to the background intensity. The initial threshold level is set to a constant value above this background level for 4X images, and to an integer number of Gaussian widths above it for 10X images, and a particle detection routine records the areas and perimeters of the nuclei. A minimum area for nuclei, dependent on the magnification used for the image, is used to reject extraneous small objects.

It is possible that two or more adjacent nuclei may be identified as one, and to resolve these nuclei, or confirm that it is a single nucleus, each object identified by the first thresholding is further examined independently. Additional thresholding and particle detection is carried out at incrementally increasing levels, until either the area of the object reaches the minimum nucleus area, in which case the object is classified as one nucleus, or multiple objects are detected, in which case the process is repeated separately with each. The perimeters of the nuclei determined by their final thresholding levels are used to locate their centers. In Fig. 5(b) the blue traces around the nuclei indicate that two cells are present, and because the nuclei in this trap are distinct, sequential thresholding beyond the initial level did not identify additional nuclei. Two overlapping nuclei from a different trap are seen in Fig. 5(e), and in this case the initial thresholding level identified a single object. Sequential thresholding was then successful in determining the presence of two nuclei, as indicated by the blue boundaries.

Despite the use of incremental thresholding, objects comprised of two overlapping nuclei may still be identified as a single nucleus, particularly when they have different intensities. The fact that these objects are typically larger than single nuclei enables their selection for further analysis. We do this by fitting ellipses to all objects with areas and perimeters exceeding particular minima, determined separately for 4X and 10X images, and searching along the major axes of the ellipses for maxima. If two maxima are discerned the object is categorized as two nuclei, and their locations recorded. This method is illustrated with the overlapping nuclei in Fig. 5(f) that were identified as a single object after thresholding. The ends of the major axis are marked with magenta dots, and the intensity along this axis is displayed in the inset. Thresholding identified the nucleus corresponding to the large peak, and intensity examination along the major axis identified the peak for the second nucleus.

Thresholding within the region of interest is also used with the fluorescent CellTracker images to locate the perimeters of the

labeled cells. A Gaussian curve is fit to the intensity histogram, and the threshold level is set an integer number of Gaussian widths above its peak. The perimeters of the objects are recorded, and nuclei with locations within these perimeters are identified as stained cells. Nuclei not found within these areas are then unlabeled cells. Fig. 5(c) is the CellTracker Green image for the trap in Fig. 5(a), and the green overlay indicates the boundaries of green-stained cells. Since the perimeter encircles both of the nuclei it is evident that both of the cells are labeled.

A similar thresholding procedure is applied to the fluorescence images of the secondary antibody to locate the perimeters of proliferating nuclei, with the level set either a fixed amount (4X images) or an integer number of Gaussian widths (10X images) above the mean background level. If the center of a nucleus is located within the perimeter of a thresholded object it is recorded as a proliferating cell. Fig. 5(d) displays the Alexa Fluor 647 infrared image for the trap in Fig. 5(a), in which the overlaid red boundary indicates that only the cell corresponding to the nucleus on the left is proliferating.

3.3 Pair Trapping Statistics

Knowledge of the number of cells of each type in every trap enabled us to evaluate, for each cell type, the fraction of traps in the array with a given cell occupancy number. For non-magnetic arrays, the suspended cells sediment into traps as random events that are independent of each other, and we therefore hypothesized that the distribution of cells in traps could be described by the Poisson probability distribution. Accordingly, for each cell type, the mean number of cells per trap was obtained using the total number of cells in the array and the total number of traps, and we compared the experimentally determined occupancy distribution to the Poisson distribution with the experimentally derived values for the mean number of cells per trap. For the majority of arrays this comparison finds the occupancy distribution to be Poisson-like, and variations from this are likely attributable to clumps of multiple cells in suspension settling into traps and to cells that settle outside of traps that adhere in nearby traps after drifting along the array's surface.

To determine the number of heterotypic pairs created by random seeding on non-magnetic arrays, we evaluated arrays seeded with green and unlabeled 3T3 cells as well as those seeded with BPASMCs and BPAECs, two cell types found in close proximity in blood vessels. Whole arrays of 24 $\times$ 80 μm^2 traps were imaged with a 4X objective, and the analysis software was used to determine the number, location, and type of cells in each trap. Every trap was manually inspected and corrected as necessary to ensure accuracy. The arrays with BPASMC/BPAEC cultures had an average of 20.1 $\pm$ 0.2% of their traps occupied by two cells (of any type) with 7.8 $\pm$ 0.1% containing heterotypic pairs (N = 13). The arrays containing green/unlabeled 3T3 cells had 25.9 $\pm$ 0.5% of their traps occupied by two cells (of any type) with 9.4 $\pm$ 0.3% containing heterotypic pairs (N = 3). In both cases these yields corresponded to up to $\sim$ 500 heterotypic pairs per array.

We also performed initial magnetic trapping experiments with permalloy arrays using green- and orange-labeled 3T3 cells as a model system, along with BPAECs and A-431 cells as a true heterotypic system. Analysis of these experiments found average pair yields similar to those of random seeding, but several magnetic arrays offered heterotypic pair yields above the highest achieved by random seeding, as high as 15% and up to a twofold enhancement over non-magnetic trapping. For example, a typical permalloy array of 24 $\times$ 80 μm^2 traps seeded with 3T3 cells had heterotypic pairs in 245 of 1,749 traps, a yield of 14.0%. We believe that the modest enhancements observed, along with the preferential trapping at opposite ends of the traps depicted in Fig. 4, are the result of magnetic interactions between the arrays and cells with attached magnetic nanowires. Thus, for magnetic arrays, cell sedimentation no longer consists of purely random events, and for this reason should not be expected to conform to Poisson statistics. Accordingly, we calculated the heterotypic pair probability using the Poisson distribution with the mean number of cells per trap for each cell type derived from the array data, and found the actual yields exceeded these theoretical values.

3.4 Analysis of Software Accuracy

Image acquisition at 4X enables large numbers of traps to be manually imaged in a short time due to the wide field of view. However, the resolution of these images is low, which increases the likelihood of inaccuracies in the software's determinations. Accurate analysis therefore requires manual inspection of each trap, a time-consuming process. Images acquired at 10X resolution possess a higher degree of detail that aids the software.

To measure the accuracy of the software with 10X magnification, we imaged 800 traps of a typical array seeded with 3T3 cells, analyzed them with the software, and manually inspected and corrected the software's determinations. These corrected determinations were then compared to those initially made by the software to ascertain the software's accuracy. Two measures of accuracy were used: the yield, defined as the percentage of traps correctly analyzed by the software, and the purity, defined as the percentage of the software's initial determinations that are correct. These accuracy measures were used to evaluate the software's success in identifying first the number of nuclei present in each trap, and subsequently the number of nuclei along with the cell type and proliferation status of each cell. Table 1 compares the success rates of the software for empty traps, traps with single cells, and traps with pairs. For traps with pairs, the most challenging category, we note a yield of 88.4% and a purity of 81.4%.

The most common software error is the misidentification of two or more touching nuclei as a single nucleus, and to gauge the extent of the effect of these errors on the software's accuracy we determined the yield and purity while excluding traps containing these potentially problematic objects. When ignoring traps with objects above the area and perimeter limits (the limits used to determine which objects would be fit to ellipses while finding the number of nuclei present in the trap) the yield for traps with two cells is increased to 92.3% while the purity is increased to 82.7%, as seen in Table 1. The ignored traps account for approximately 10–15%, and thus these improved success rates are still based on large numbers of traps.

Lastly, as another option, we used the software to manually inspect only the traps with objects above the area and perimeter

Table 1 The success rate of the analysis software used with 10X images, as measured by yield and purity. Empty traps, trap with single cells, and traps with cell pairs are considered, and three analysis conditions are evaluated: (1) analyzing all objects, regardless of size, (2) analyzing only objects below area and perimeter limits of 550 pixels and 90 pixels, respectively, and (3) analyzing only objects below these limits and then manually inspecting the larger objects and correcting as necessary

	Empty Traps	Singles	Doubles
Yield			
Including Large Aggregates			
Nuclei only	99.1	97.6	92.9
Nuclei, cell type, & BrdU	99.1	93.7	88.4
Excluding Large Aggregates			
Nuclei only	99.1	97.0	97.2
Nuclei, cell type, & BrdU	99.1	94.0	92.3
w/ Manual Inspection of Large Aggregates Only			
Nuclei only	99.1	97.6	97.5
Nuclei, cell type, & BrdU	99.1	95.1	92.9
Purity			
Including Large Aggregates			
Nuclei only	96.6	93.9	85.6
Nuclei, cell type, & BrdU	96.6	90.1	81.4
Excluding Large Aggregates			
Nuclei only	96.6	97.6	87.1
Nuclei, cell type, & BrdU	96.6	94.6	82.7
w/ Manual Inspection of Large Aggregates Only			
Nuclei only	96.6	98.1	87.9
Nuclei, cell type, & BrdU	96.6	95.8	83.7

limits. After correcting the misidentifications in just this subset we again determined the yield and purity based on an evaluation of all traps. This approach offers the ability to ensure the accuracy of the traps most likely to be misidentified, while avoiding the manual inspection of those that are not, leading to a modest improvement of the yield to 92.9% and the purity to 83.7% (Table 1).

3.5 BPAEC-BPASMC Proliferation Study

We have demonstrated the use of the array trapping technique and analysis system in experiments that probe the effects of pairwise cell contact on proliferation rates. To do so we used endothelial and smooth muscle cells that form the inner lining and interior structure of blood vessels, respectively, and are naturally in close proximity *in vivo*. Cell-cell interactions between these cell types have been studied previously in systems that cultured monolayers of each type on opposite sides of a porous membrane,[27,28] but this environment is unable to control the number of cells of the same type contacted, and heterotypic contacts are made by cytoplasmic projections extending through pores several microns in length. Our method allows for a much greater degree of contact between the cells, and eliminates the potentially confounding effects of contact with additional surrounding cells. It has been previously shown that the number of cell-cell contacts, and the spatial location of those contacts, can impact cell behaviors including cell proliferation.[20,32] Thus, better control over such contact could be useful in a number of settings.

The BPAECs and BPASMCs were mixed and randomly seeded onto arrays, producing both homotypic and heterotypic pairs. Arrays of small (14 × 70 μm^2) and large (24 × 80 μm^2) traps were imaged at 4X, analyzed, and corrected by manual inspection. Pairs of cells confined to the traps were counted and included in the pair yield data in Section 3.3. Heterotypic yields varied between 6.3% (338 pairs) and 9.8% (527 pairs) for arrays of small traps, and between 5.3% (237 pairs) and 10.0% (442 pairs) for arrays of large traps. Homotypic yields varied between 9.0% (487 pairs) and 15.2% (817 pairs) for small-trap arrays, and between 6.9% (310 pairs) and 14.6% (644 pairs) for large-trap arrays.

We measured the proliferation rates of BPAECs and BPASMCs in both hetero- and homotypic pairs, as defined by

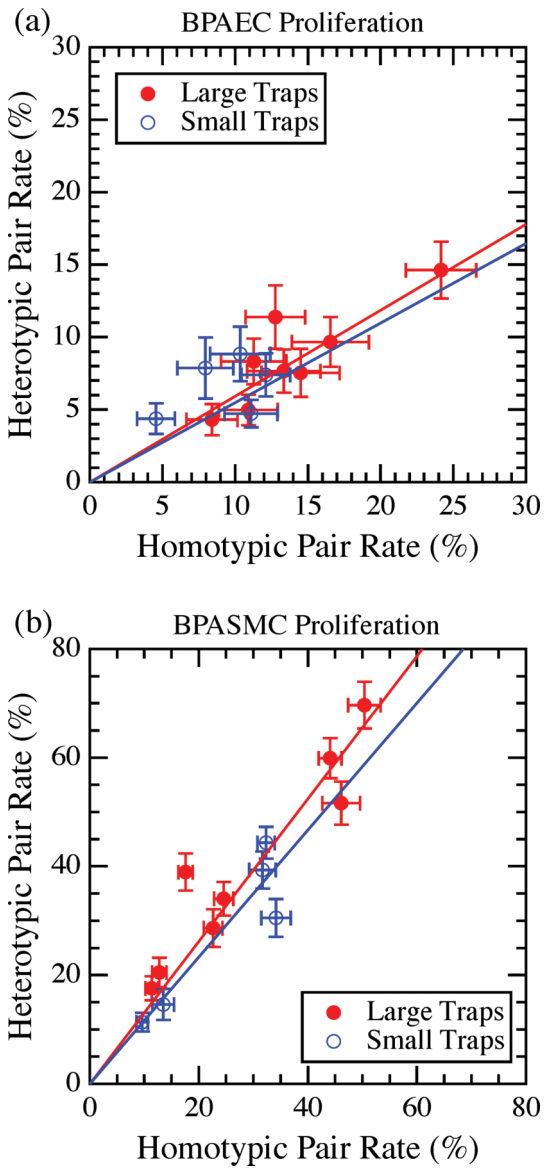

Fig. 6 (a) Proliferation rates of BPAECs in heterotypic pairs with BPASMCs as a function of BPAEC proliferation in homotypic pairs. (b) Proliferation rates of BPASMCs in heterotypic pairs with BPAECs as a function of BPASMC proliferation in homotypic pairs. Data shown for both large and small cell trap sizes.

entry into S phase, with a BrdU assay. The proliferation rate for the BPAECs was less than 25% regardless of pair type. A comparison of BPAEC proliferation rates in homotypic and heterotypic pairs determined that in any particular experiment, the BPAECs consistently had higher proliferation rates when in the homotypic configuration, suggesting that contact with the BPASMCs may inhibit their proliferation. These data are displayed in Fig. 6(a), in which heterotypic proliferation rates of arrays are plotted as a function of homotypic rates. Linear fits to the data points for small and large traps have slopes of 0.59 $\pm$ 0.01 and 0.55 $\pm$ 0.01, respectively. Calculations determined the average ratio of proliferating BPAECs in hetero- to homotypic pairs to be 0.58 $\pm$ 0.08 (small traps) and 0.58 $\pm$ 0.05 (large traps), in good agreement with the fit. We note that the proliferation decrease observed is in contrast to a study that measured proliferation of BPAECs cultured on a membrane with and without BPASMCs on the opposite side, which concluded that contact with the BPASMCs had no effect on BPAEC proliferation.[28]

The BPASMCs had higher overall proliferation rates than the BPAECs, although considerable variation was observed from experiment to experiment, ranging as low as 10% in homotypic pairs in a small-trap array to 70% in heterotypic pairs in an array of large traps. A comparison of BPASMC proliferation in the two configurations showed that those in heterotypic pairs consistently had significantly higher proliferation rates than those in homotypic pairs, and that the ratio of hetero- to homotypic BPASMC proliferation rates is greater than unity with just a single exception. These data are plotted in Fig. 6(b), and linear fits to these data have slopes of 1.17 $\pm$ 0.01 (small traps) and 1.31 $\pm$ 0.01 (large traps). The average ratios for BPASMCs in small and large traps were found to be 1.17 $\pm$ 0.07 and 1.37 $\pm$ 0.05, respectively, also in agreement with the fits. The observed BPASMC proliferation rates indicate that contact with endothelial cells promotes increased proliferation of BPASMCs, a finding that is in agreement with the previously cited cells-on-membrane study.

4 Conclusions

We have introduced a versatile technique that makes use of lithographic patterning of thin metal films to form arrays of heterotypic and homotypic cell pairs on substrates. Using this approach, we showed that cell-cell interactions can influence the proliferation rates of endothelial and smooth muscle cells. Interestingly, endothelial cells are inhibited in the presence of smooth muscle cells whereas smooth muscle cells appear to be less affected by endothelial cells, suggesting that in a co-culture of both cell types, smooth muscle cells would ultimately dominate the culture. These findings illustrate the potential utility of these methods in investigating the role of cell-cell interactions in controlling cell function.

The approach offers a great deal of flexibility due to the variety of parameters that can be altered. First, the size of the traps and intertrap spacing can be readily changed, and patterning over wide areas is easily achieved and is capable of producing large numbers of cell pairs. We have shown that cells can be deposited on the array and allowed to position themselves through their interactions with the chemically treated substrate. The array fabrication process also enables the incorporation of additional layers of material in the thin film, and by adding magnetic layers we have created traps with magnetic poles that enable the use of magnetic forces to guide cells with magnetic particles to opposite trap ends. We selected permalloy for this work, but the materials used and the thickness and number of layers can each be chosen to tailor the magnetic characteristics of the array for a particular application. By using magnetic trapping, we observed a modest increase in heterotypic yield over randomly seeding cells onto the traps, and would anticipate that modifications to further increase the traps' remanent magnetization may further increase this effect. Although not all array sites contain heterotypic pairs, both the magnetic and nonmagnetic cell trapping methods produce several hundred heterotypic pairs per array, and each sample in turn has four arrays. This results in ample numbers of pairs for analysis, and we have demonstrated this in experiments that measure the influence of contact between different cell types on their proliferation rates.

We have also developed analysis software that works in tandem with the arrays of trapped cells. This tool makes possible the acquisition of data from multiple optical channels from every trap in an array, and enables ready analysis of many hundreds of cell pairs. The software has been used here with lower magnification images, but it can be easily adapted to other magnifications. Furthermore, it can be used to extract data from images of additional channels, and is capable of identifying labeled objects of different sizes beyond those we have explored. The degree of automation can also be adjusted to suit the needs of a given experiment. For cases that demand a high level of accuracy it is possible for the user to inspect the software's findings and intervene when traps are incorrectly analyzed, but this can be bypassed in situations that do not require as high a level of accuracy and efficiency is desired. In either case the software provides a thorough analysis of the array.

We anticipate that this combination of flexible cell patterning and analysis should facilitate numerous *in vitro* experiments on cell-cell interactions. As illustrated here, the interactions between endothelial and smooth muscle cells provide one example for such future work. Beyond that, the study of complex multi-cellular processes such as those that occur in development and physiological adaptation often involve specific induction events involving contact-mediated cell-cell signaling between two cell types, such as occurs with Notch/Delta,[40] cadherin receptors,[41] neuronal synapses,[42] and immunological synapses.[43] Using our approach to restrict interactions to pairs of cells isolates such interactions from the many other possible complex communication circuits that might influence development in multi-cellular assemblies, and therefore simplifies their study. For example, the events associated with tumor vascularization and the evolution of the tumor microenvironment[44] are driven by a myriad of both heterotypic and homotypic interactions between epithelial, endothelial, smooth muscle and stromal cells, as well as with pericytes of the blood vessels that feed the tissue. Sorting out the influence of these interactions on cancer progression has proven difficult, and could potentially benefit from the detailed information on pair-wise cellular processes that our approach can provide.

Acknowledgements

This work was supported in part by NIH Grant R21-CA128622. CRC was supported by a NSF IGERT fellowship. We thank Leyi Zhu for assistance with MFM measurements.

References

1 R. Singhvi, A. Kumar, G. P. Lopez, G. N. Stephanopolous, D. I. Wang, G. M. Whitesides and D. E. Ingber, *Science*, 1994, **264**, 696–698.
2 B. C. Wheeler, J. M. Corey, G. J. Brewer and D. W. Branch, *J. Biomech. Eng.*, 1999, **121**, 73–79.
3 J. L. Tan, C. M. Nelson and C. S. Chen, *Tissue Eng.*, 2004, **10**, 865–872.
4 C. P. Tan, B. R. Seo, D. J. Brooks, E. M. Chandler, H. G. Craighead and C. Fischbach, *Integr. Biol.*, 2009, **1**, 587–594.
5 M. Tanase, E. J. Felton, D. S. Gray, A. Hultgren, C. S. Chen and D. H. Reich, *Lab Chip*, 2005, **5**, 598–605.
6 W. Liu, N. Dechev, I. G. Foulds, R. Burke, A. Parameswaran and E. J. Park, *Lab Chip*, 2009, **9**, 2381–2390.
7 M. F. Lai, C. Y. Chen, C. P. Lee, H. T. Huang, T. R. Ger and Z. H. Wei, *Appl. Phys. Lett.*, 2010, **96**, 183701.
8 P. Kauffmann, A. Ith, D. O'Brien, V. Gaude, F. Boué, S. Combe, F. Bruckert, B. Schaack, N. M. Dempsey, V. Haguet and G. Reyne, *Lab Chip*, 2011, **18**, 3153–3161.
9 M. Frenea-Robin, H. Chetouani, N. Haddour, H. Rostaing, J. Lafloret and G. Reyne, *Conference Proceedings – IEEE Engineering in Medicine and Biology Society*, **2008**, 3360–3363.
10 R. Pethig and G. H. Markx, *Trends in Biotechnol.*, 1997, **15**, 426–432.
11 D. R. Albrecht, V. L. Tsang, R. L. Sah and S. N. Bhatia, *Lab Chip*, 2005, **5**, 111–118.
12 J.-P. Frimat, M. Becker, Y.-Y. Chiang, U. Marggraf, D. Janasek, J. G. Hengstler, J. Franzke and J. West, *Lab Chip*, 2011, **11**, 231–237.
13 I. K. Zervantonakis, C. R. Kothapalli, S. Chung, R. Sudo and R. D. Kamm, *Biomicrofluidics*, 2011, **5**, 013406.
14 D. Choquet, D. P. Felsenfeld and M. P. Sheetz, *Cell*, 1997, **88**, 39–48.
15 R. K. Pirlo, Z. Ma, A. Sweeney, H. Liu, J. X. Yun, X. Peng, X. Yuan, G. X. Guo and B. Z. Gao, *Rev. Sci. Instrum.*, 2011, **82**, 013708.
16 C. M. Nelson and C. S. Chen, *FEBS Lett.*, 2002, **514**, 238–242.
17 D. S. Gray, J. L. Tan, J. Voldman and C. S. Chen, *Biosens. Bioelectron.*, 2004, **19**, 1765–1774.
18 Z. Yin, D. Noren, C. J. Wang, R. Hang and A. Levchenko, *Mol. Syst. Biol.*, 2008, **4**, 232.
19 C. M. Nelson, D. Pirone, J. L. Tan and C. S. Chen, *Mol. Biol. Cell*, 2004, **15**, 2943–2953.
20 C. M. Nelson and C. S. Chen, *J. Cell Sci.*, 2003, **116**, 3571–3581.
21 R. A. Desai, L. Gao, S. Raghavan, W. F. Liu and C. S. Chen, *J. Cell Sci.*, 2009, **122**, 905–911.
22 A. Armulik, A. Abramsson and C. Betsholtz, *Circ. Res.*, 2005, **97**, 512–523.
23 E. Hatten, *Trends Neurosci.*, 1990, **13**, 179–184.
24 A. Ito, T. Kiyohara, Y. Kawabe, H. Ijima and M. Kamihira, *J. Biosci. Bioeng.*, 2008, **105**, 679–682.
25 M. Nikkhah, J. S. Strobl, E. M. Schmelz, P. C. Roberts, H. Zhou and M. Agah, *Biomaterials*, 2011, **32**, 7625–7632.
26 D. I. Axel, R. Riessen, A. Athanasiadis, H. Runge, G. Koveker and K. R. Karsch, *J. Mol. Cell Cardiol.*, 1997, **29**, 2967–2978.
27 M. F. Fillinger, L. N. Sampson, J. L. Cronenwett, R. J. Powell and R. J. Wagner, *J. Surg. Res.*, 1997, **67**, 169–178.
28 O. J. Imegwu, I. Entersz, A. M. Graham and G. B. Nackman, *J. Surg. Res.*, 2001, **98**, 85–88.
29 D. Wright, B. Rajalingam, S. Selvarasah, M. R. Dokmeci and A. Khademhosseini, *Lab Chip*, 2007, **7**, 1272–1279.
30 X. Cheng, Y. Wang, Y. Hanein, K. F. Böhringer and B. D. Ratner, *J. Biomed. Mat. Res. A*, 2004, **70**, 159–168.
31 S. J. Bidarra, C. C. Barrias, M. A. Barbosa, R. Soares, J. Amedee and P. L. Granja, *Stem Cell Res.*, 2011, **7**, 186–197.
32 D. S. Gray, W. F. Liu, C. J. Shen, K. Bhadriraju, C. M. Nelson and C. S. Chen, *Exp. Cell Res.*, 2008, **314**, 2846–2854.
33 K. Terao, Y. Kitazawa, R. Yokokawa, A. Okonogi and H. Kotera, *Lab Chip*, 2011, **11**, 1507–1512.
34 S. N. Bhatia, U. J. Balis, M. L. Yarmush and M. Toner, *FASEB J.*, 1999, **13**, 1883–1900.
35 A. M. Skelley, O. Kirak, H. Suh, R. Jaenisch and J. Voldman, *Nat. Methods*, 2009, **6**, 147–152.
36 M. Mrksich, L. E. Dike, J. Tien, D. E. Ingber and G. M. Whitesides, *Exp. Cell Res.*, 1997, **235**, 305–313.
37 A. Hultgren, M. Tanase, E. J. Felton, K. Bhadriraju, A. K. Salem, C. S. Chen and D. H. Reich, *Biotech. Prog.*, 2005, **21**, 598–605.
38 J. Miyakoshi, *Prog. Biophys. Mol. Bio.*, 2005, **87**, 213–223.
39 A. Umeno and S. Ueno, *IEEE Trans. Nanobiosci.*, 2003, **2**, 26–28.
40 E. C. Lai, *Development*, 2004, **131**, 965–973.
41 B. M. Gumbiner, *Nat. Rev. Mol. Cell Biol.*, 2005, **6**, 622–634.
42 Z. Li and M. Sheng, *Nat. Rev. Mol. Cell. Biol.*, 2003, **4**, 833–841.
43 P. Friedl, A. Th. den Boer and M. Gunzer, *Nat. Rev. Immunol.*, 2005, **5**, 532–545.
44 M. J. Bissell and D. Radisky, *Nat. Rev. Cancer*, 2001, **1**, 46–54.

